Scientific Reports

https://doi.org/10.1038/s41598-026-50739-0

Article in Press

Long term mangrove dieback and recovery at Godorya Marine Protected Area in the Gulf of Aden under climate variability

Received: 6 September 2025

Accepted: 23 April 2026

Published online: 26 April 2026

Cite this article as: Ahmed M.M., Awaleh M.O., Ibrahim A.Y. *et al.* Long term mangrove dieback and recovery at Godorya Marine Protected Area in the Gulf of Aden under climate variability. *Sci Rep* (2026). https://doi.org/10.1038/s41598-026-50739-0

Moussa Mahdi Ahmed, Mohamed Osman Awaleh, Asma Yacin Ibrahim, Omar Assowe Dabar, Mahamoud Ali Chirdon, Moussa Mohamed Waberi, Abdi-Basid Ibrahim Adan & Nasri Hassan Ibrahim

Long term mangrove dieback and recovery at Godorya Marine Protected Area in the Gulf of Aden under climate variability

Moussa Mahdi Ahmed[a*], Mohamed Osman Awaleh[b], Asma Yacin Ibrahim[a], Omar Assowe Dabar[a], Mahamoud Ali Chirdon[a], Moussa Mohamed Waberi[a], Abdi-Basid Ibrahim Adan[a], Nasri Hassan Ibrahim[a].

[a]Observatoire Régional de Recherche sur l'Environnement et le Climat (ORREC), Centre d'Etudes et de Recherches de Djibouti (CERD), Djibouti, Route de l'aéroport, Djibouti City, B.P. 486, Djibouti
[b]Institut des Sciences de la Terre (IST), Centre d'Etudes et de Recherches de Djibouti (CERD), Route de l'aéroport, Djibouti-ville B.P. 486, Djibouti

*** Corresponding authors.**
E-mail address: moussa.mahdi@chemist.com (Moussa Mahdi Ahmed)

Abstract

Mangrove ecosystems along arid and semi-arid coastlines are susceptible to climate variability and hydrodynamic change. Here, we present the first comprehensive multi-decadal assessment of mangrove canopy dynamics in the Red Sea–Gulf of Aden over the period 1987–2022. Canopy condition was assessed using NDVI as a proxy, while mangrove cover was derived from supervised classification of satellite imagery. NDVI reached a minimum of 0.21 during the 2009 drought and increasing to 0.45 by 2022 during wet years. A multi-decadal mangrove cover record revealed a 30.5% loss in mangrove cover between 1987–2012 followed by partial recovery (+25.3%) between 2015–2022. Correlation analyses show significant relations between sea level anomaly and mangrove cover ($r = 0.62$, $p < 0.001$), and between rainfall and NDVI ($r = 0.48$, $p < 0.01$). Using detrended anomaly-based multiple regression, we show that mangrove dynamics are primarily controlled by sea level anomaly, rainfall, and temperature. Sea level anomaly emerges as the dominant driver of mangrove extent, while vegetation greenness reflects combined hydroclimatic influences, highlighting distinct controls on structural and physiological ecosystem responses. Our findings underscore the importance of hydrological processes in shaping mangrove resilience in the Red Sea–Gulf of Aden.

Keywords: Mangroves; dieback; normalized difference vegetation index; sea level anomaly; Gulf of Aden

1. Introduction

Mangroves are among the most productive ecosystems on Earth and provide a wide range of ecosystem services, including carbon sequestration[1,2], shoreline stabilization[3,4], protection from storm surges and tsunamis[5,6], sediment trapping[7], natural remediation of coastal environments[8], and essential nursery habitats for invertebrates and juvenile fish[9]. Mangrove systems occurring in dry ecoregions such as the Red Sea and the Gulf of Aden are typically less structurally complex than tropical mangrove systems, but perform similar ecological functions[10]. Within these arid environments, mangroves are additionally subject to anthropogenic pressures such as over-cutting[11], grazing[12,13] and pollution[14]. Extensive damage has already been documented at many sites, and only stands located on remote or protected islets where camels do not have access appear to remain relatively intact[13]. Mass mortality of mangrove trees has been reported along the southern coasts of Yemen and Sudan, and on the Gulf of Aden coast of Djibouti, where extensive areas have disappeared[15].

Climatic variables such as sea surface temperature, air temperature, rainfall, and wind patterns are shaped by ocean-atmosphere interactions[16]. Numerous climatic drivers are recognized as important factors influencing mangrove dynamics at local and regional scales[17-19]. While the climatic drivers can include a variety of factors, temperature, salinity, and rainfall consistently emerge as the most important abiotic factors affecting mangrove distribution and condition in mangrove forests. Alterations in these abiotic factors can disrupt ecosystem services, and climate change has therefore emerged as a major driver of stress and degradation in mangrove ecosystems[20]. These pressures have been made worse by reduced rainfall and runoff, which compromise the vegetation’s ability to trap sediments[21]. The El Niño-Southern Oscillation (ENSO) represents a dominant mode of interannual climate variability across East Africa, influencing sea level, rainfall, and temperature regimes[22-24]. The Indian Ocean Dipole (IOD) can further modulate regional rainfall, wind regimes,

and ocean conditions. In vulnerable systems, relatively small changes in sea level or freshwater input, can result in pronounced shifts in mangrove persistence or failure[19,25,26]. Understanding these teleconnections is important for developing predictions and expectations for ecosystem responses and management and restoration of climatically vulnerable coastlines. Furthermore, extreme climate events such as the 1997–1998 El Niño have been associated with substantial sediment redistribution and widespread mangrove mortality in the region as reported by the Regional Organization for the Conservation of the Environment of the Red Sea and Gulf of Aden[15]. Extreme sea surface temperature anomalies during El Niño events may further alter hydrodynamic conditions (e.g., anomalously low sea levels), increasing exposure of mangrove pneumatophores to desiccation.

Mapping and monitoring the spatial distribution and dynamics of the canopy of mangrove forests, and quantifying their loss and regrowth through time are important for conserving and sustainably managing mangrove forests[27]. However, in Djibouti and the broader Red Sea–Gulf of Aden region, long-term and site-specific assessment programs have been slow to develop. Few studies have investigated the long-term, systematic change in mangrove canopy through time under arid zone settings[28-30]. Recent advances in remote sensing now allow mangrove ecosystems to be monitored and managed[31]. In particular, Landsat imagery provides a consistent and continuous multi-decadal record that can be assessed against available environmental datasets to evaluate change[32]. The distinct spectral properties of mangroves enable not only the mapping of their spatial extent, but also the characterization of canopy structure and condition[33,34]. Nevertheless, much of the existing literature has focused on localized areas or single disturbance events, failing to capture prolonged trajectories of dieback and recovery related to climatic drivers (rainfall, temperature, sea level, etc…)[35]

To address this knowledge gap for mangroves at the arid margin which remains understudied despite its high vulnerability to climate variability,

this study presents the first multi-decadal assessment of mangrove dynamics at the Godorya Marine Protected Area, providing regional context for mangrove change. Using three decades (1987–2022) of Landsat satellite images, we assessed the Normalized Difference Vegetation Index (NDVI) as a proxy for canopy condition to detect spatial and temporal variations. Accordingly, this study was designed with three objectives: (i) to quantify long-term changes in mangrove canopy cover, (ii) to assess patterns of degradation and regrowth using NDVI and spatial clustering approaches, and (iii) to examine relationships between mangrove metrics and climatic variables.

2. Methods

2.1 Site Study

The Godorya mangrove ecosystem (**Figure 1**), located in the northern coastal plain of the Obock region (Republic of Djibouti) along the Red Sea near the Bab El-Mandeb Strait, represents one of the most arid and marginal mangrove ecosystems in the Western Indian Ocean[36]. The site is characterized by a tropical arid climate, with annual rainfall averaging around 130 mm and extreme temperatures ranging from 22–30 °C in winter to 33-45 °C in summer, conditions that drive high evapotranspiration and salinity stress. The geomorphology consists of a shallow sandy–muddy substrate interspersed with elevated coral platforms and halomorphic soils which supports a mosaic of hydromorphic depressions, salt-encrusted tannes, and tidal channels that are submerged by approximately 15–20 cm of water during spring tides[15]. Vegetation cover is dominated by Avicennia marina, which occupies the landward fringe. While *Rhizophora mucronata*, *Ceriops tagal*, and *Bruguiera gymnorhiza* are confined to the tidal channels and inner canopy zones[37]. The surrounding terrestrial matrix consists of halophytic shrubs (*Suaeda fructicosa*), sparse Acacia steppe, and dune vegetation, which is heavily degraded by overgrazing. Ecologically, the Godorya mangroves provide critical nursery habitat for fishes and crustaceans[38], and host diverse

avifauna[39,40], including migratory waders and piscivorous raptors[41], while supporting local artisanal fisheries and pastoral livelihoods.

2.2 Datasets

Data were compiled into a multi-decadal archive of 73 cloud-free multispectral satellite scenes from 1987 to 2022 acquired by Landsat 5 TM, Landsat 7 ETM+, and Landsat 8 OLI sensors (Path 166, Row 52). All datasets were obtained from the USGS Earth Explorer and were Level-2 surface reflectance products derived from LEDAPS for TM/ETM+ and LaSRC for OLI (WGS84 UTM Zone 38N). To minimize cloud and phenological noise, all scene identifiers, sensor types (TM, ETM+, OLI), months, and years are listed in **Table SI1**. Images were primarily acquired during late summer (July–September), minimizing cloud contamination and ensuring comparable seasonal conditions.

Monthly rainfall was retrieved from the Climate Hazards group InfraRed Rainfall and Station data (CHIRPS) dataset, which merges satellite observations with in-situ gauge records at 0.05° (~5 km) spatial resolution, from 1981 to the present. Rainfall data were extracted from CHIRPS pixels centered on Obock and Djibouti City, a long-term national reference station[23].

Sea level anomaly (SLA) data were acquired from multi-mission satellite altimetry products beginning in 1992 (TOPEX/Poseidon, Jason-1 to Jason-3, Sentinel-6MF, Envisat) and distributed by NOAA's Laboratory for Satellite Altimetry. The SLA was then barometrically corrected using the inverted barometer method, which adjusts for variations in atmospheric pressure. Air temperature metrics (2 m minimum, mean, and maximum temperatures) were extracted from the ERA5 reanalysis, representing monthly estimates of atmospheric variables at 0.25° spatial resolution[25].

Indices of large-scale climate variability were sourced from the NOAA Physical Sciences Laboratory. The Niño 3.4 and the Dipole Mode Index were used to represent the El Niño-Southern Oscillation and Indian Ocean Dipole respectively[26].

2.3 Methodology

Normalized Difference Vegetation Index (NDVI) was defined using surface reflectance values, as NDVI = (NIR–R) / (NIR+R) [27]. NDVI was computed for Landsat 5 TM and 7 ETM+ using the red (Band 3: 0.63–0.69 µm) and NIR (Band 4: 0.78–0.90 µm) channels, and for Landsat 8 OLI using the red (Band 4: 0.64–0.67 µm) and NIR (Band 5: 0.85–0.88 µm) channels (Table SI2). For Landsat 8 OLI, the index was derived from the red (Band 4: 0.64–0.67 µm) and near-infrared (Band 5: 0.85–0.88 µm) bands. In order to ensure temporal consistency, we adjusted Landsat 5 TM and 7 ETM+ data to Landsat 8 OLI using the conversion coefficients reported by Roy, et al. [42].

Landsat pixels in arid mangrove settings often represent mixed surfaces (vegetation, salt crusts, sediment, shallow water). All data were produced using Level-2 surface reflectance datasets (LEDAPS and LaSRC) and NDVI was calculated using consistent mangrove masks for the specific bands in order to prevent inter-sensor discontinuities. A sustained high NDVI (≥ 0.45) was interpreted as areas of relatively high and stable canopy greenness. Low mean NDVI values (≤ 0.25) were interpreted as persistently low canopy greenness consistent with degraded or sparse canopy conditions or dynamic fringe zones.

The two-step approach to create a mangrove canopy map included a supervised land cover classification that identified mangrove vegetation in relation to water and bare or salt-affected substrates based on satellite imagery[45]. The classifier used was a Maximum Likelihood Classifier (MLC), with sample data collected for the three land-cover classes. The second step identified the mangrove canopy density by calculating the NDVI. This was used to distinguish areas of low-density or stressed mangrove canopies from those with higher density and health. The NDVI classifications were not separate land cover categories but rather indicator of the mangrove internal condition.

Training sets were adjusted to be consistent with temporal patterns of phenology and spectral characteristics to account for variability among

sensors (TM, ETM+, and OLI), thus classification accuracy was assessed using reference data that are independent of the Landsat satellite imagery (Google Earth) and/or in situ GPS control points established by the field survey. The use of these control points was limited to assessment of classification accuracy, as all Landsat scenes were orthorectified Level-2 surface reflectance products. An illustrative example of the supervised classification and validation procedure is provided in **Figure SI1**.Classification accuracy was assessed using independent high-resolution imagery (e.g., Google Earth) and in situ GPS validation points (10 points per class) collected during field surveys, referenced to the three land-cover classes (mangrove, water, bare substrate)[46]. Accuracy measures included overall accuracy and Kappa coefficients, which ranged from 87.5% to 94.4% and always exceeded 0.81 (**Table SI3**). Omission and commission errors were considered acceptable error rates for long-term mangrove monitoring, although omission error was higher in years with extreme stress (2002–2003) impacting sparsely canopied counts[23].

We performed a non-parametric trend analysis, namely Mann-Kendall and Sen's slope tests on NDVI, mangrove cover and climate variables with statistical significance evaluated at $p \leq 0.05$. NDVI anomalies were computed as the deviation of annual mean NDVI from the long-term mean NDVI ((ΔNDVI), 1987–2022) divided by the standard deviation within the annual mangrove mask, while minimizing contamination due to mixed pixels containing non-mangrove vegetation. Local Moran's I, following Bera and Das Chatterjee [47], was computed on ΔNDVI to identify spatial clustering of canopy stress and recovery. We then determined the level of statistical significance and categorized pixels in one of four standard LISA categories (high-high; low-low; high-low; low-high; not significant).

Mangrove cover and NDVI were assessed using Pearson correlations with selected climate variables (Niño 3.4, IOD, rainfall and temperature) to quantify linear associations ($p \leq 0.05$). All climate–mangrove relationships were evaluated at the annual scale using common years (1992 to 2022).

To assess the independent effects of hydroclimatic drivers on vegetation dynamics, a multiple linear regression framework was applied to detrended time series. Variables were first detrended and expressed as standardized anomalies, it isolates interannual variability and allows for a more robust evaluation of the relationships between environmental drivers and vegetation response. Two separate regression models were developed to analyze (i) vegetation greenness (NDVI) and (ii) mangrove area as follows:

$$NDVI' \text{ or Mangrove area} = \beta + k_1\beta_1 + k_2\beta_2 + \ldots\ldots + k_n\beta_n + \varepsilon$$

where $NDVI'$ and $\text{Mangrove Area}'$ represent detrended anomaly time series, β is the intercept, k_i are regression coefficients, and ϵ is the residual error term. The predictors β_i correspond to detrended anomalies such as rainfall, mean air temperature, and sea level anomaly, respectively. Model performance was evaluated using the coefficient of determination (R^2), adjusted R^2, and the statistical significance of regression coefficients. Multicollinearity among predictors was assessed using the Variance Inflation Factor (VIF), and only variables with acceptable collinearity levels were retained in the final models.

3. Results

3.1 Mangrove cover dynamics

Using supervised classification of the multi-decadal Landsat imagery, we identified pronounced fluctuations in mangrove extent within the Godorya Marine Protected Area (MPA) over the period 1987 to 2022. The temporal evolution of mangrove cover is reported in **Figure 2** with two statistically significant breakpoints ($p \leq 0.05$) in 1997 and 2014 indicating a major shift in ecosystem dynamics. The trajectory is distinctly nonlinear and can be partitioned into three phases is observed, a gradual decline (1987–2003), a plateau where there was partial dieback (2003–2012), and a regrowth phase (after 2015). The most pronounced decline in mangrove extent occurred around 2001, corresponding to the minimum recorded mangrove area. The non-parametric trend analysis of mangrove cover was conducted

and reported in **Table SI4**, results indicate a statistically significant statistically significant long-term increase in mangrove extent over the entire time period (τ=0.27, p=0.04) and a positive rate of change per year of + 1.76 ha yr^{-1}.

Spatial patterns of mangrove cover change in the Godorya Marine Protected Area for decadal thresholds are reported in **Figure 3**. During the first decade, (1987-1997; **Figure 3a)** changes were limited, with 17 ha of gain and 9 ha of loss corresponding to 5.3% gain and -2.8% loss relative to the initial mangrove extent. The majority of the mangrove cover remained unchanged (296 ha; 91.9 %), this stability suggests a relatively resilient mangrove cover. In contrast, the second decade (1997–2007) represented in **Figure 3b** shows a substantial decline, with 54 ha loss (-20.9%) compared to only 20 ha (7.8%) of gain. The unchanged area decreased to 204 ha (71%) significantly compared to period 1987–1997 indicating a widespread spatial reorganization. The third decade (2007–2017) reported in **Figure 3c** and reflects a growth period; with a total of 93 hectares of increase and only 11 hectares of decrease, corresponding to 36.5% gain and -4.3% loss relative to the mangrove extent. With 212 ha (59.2%) unchanged cover corresponding to rapid regrowth dynamics. Finally, the last phase (2017-2022; **Figure 3d**) is characterized by relative stability, with 19 ha of growth and only a very small decline of around 6 ha, equivalent to 7.4% gain and -2.3% loss. The majority of the mangrove units (239 ha; 90.7%) remained unchanged, suggesting consolidation of the recovery phase.

3.2 Mangrove canopy condition dynamics (NDVI)

In contrast to structural changes in mangrove extent, the NDVI time series derived from the classified mangrove extent showed clear interannual fluctuations in canopy greenness over the multi-decadal record (**Figure 2**). Non-parametric trend analysis using the Mann–Kendall test indicates no significant monotonic trend over the 1987-2022 period (τ=0.02, p=0.88) suggesting that canopy condition follows fluctuates over time.

During the period of 1997–2009, average NDVI values declined from 0.46 in 1997 to a minimum of 0.21 in 2001, likely reflecting environmental stress associated with extreme climatic events, potentially linked to the 1997–1998 El Niño. This time period corresponds to the lowest NDVI values recorded, consistent with reduced photosynthetic activity under prolonged drought and low sea level conditions. These NDVI values approached the lower range commonly reported for sparse arid *Avicennia marina* stands. Accordingly, NDVI < 0.25 was treated here as an operational proxy for very low photosynthetic activity rather than a physiological mortality threshold[11].

To illustrate temporal changes in canopy condition, we used a Sankey diagram (see **Figure SI2**) to synthesize transitions among canopy condition classes based on NDVI values. Between 1997 and 2012, canopy degradation was dominated by transitions from moderate to low NDVI classes (109.1 ha), whereas recovery between 2012 and 2016 was characterized by transitions from low to high NDVI. The breakpoint identified in 2014 marks a transition toward recovery, after which NDVI values increase and stabilize (0.45–0.50) thereafter, indicating improved canopy condition. During 2016–2022, an increase in class persistence was observed, characterized by numerous transitions within the same High-High condition as well as many transitions within the same Low-Low condition.

Despite the absence of a significant trend at the aggregated scale (mean NDVI); however, there is considerable spatial variability in NDVI at the pixel level (see Figure 4). Sen's slope estimates (**Figure 4a**) reveal that 68% of all mangrove pixels exhibited positive NDVI trends, while the remaining 32% exhibited negative or near-stable trends. The Mann-Kendall test (**Figure 4b**) further indicated that approximately one-third of all pixels had a statistically significant positive trend ($p<0.05$). Positive trends corresponding to greening were largely confined to the north and center sectors, indicating coordinated canopy recovery. In contrast, negative trends were found in the southern zone, which indicates persistent

mangrove health degradation in these areas. The Local Moran's I analysis (**Figure 4c-4d)** provides additional insight into the spatial organization of canopy condition during contrasting ecosystem states. During the degradation regime (2012, **Figure 4c**), extensive low-low clusters were observed in the southern portion of the study area indicating spatially coherent areas experiencing low NDVI values and persistent canopy condition stress. Conversely, during the recovery regime (2022, Figure 4d), extensive high-high clusters were observed in both the northern and central sectors of the study area indicating spatially coherent areas with high NDVI values associated with canopy condition recovery. The comparison between these two years (2012, 2022; **Figure SI3**) highlights a transition from spatially structured degradation to clustered recovery, consistent with the regime shifts identified in the NDVI time series.

3.3 Relationships with hydroclimatic drivers

To contextualize the climate-mangrove relationships, **Figure 5** illustrates temporal variability over key climatic and oceanic drivers. SLA showed a marked increase after 2005 (**Figure 5a**) consistent with non-parametric trend analysis (**Table SI4**) indicating a strong positive monotonic trend in sea level anomaly ($\tau = 0.56$, $p \leq 0.0001$; Sen's slope = 0.0037 yr^{-1}). Mean air temperature (**Figure 5b**) shows a statistically significant upward trend over 1987–2022 (Mann–Kendall $\tau = 0.60$, $p \leq 0.0001$), with a positive Sen's slope of +0.04 °C·yr^{-1}, indicating progressive warming. In contrast, Niño 3.4 illustrated in **Figure 5c** exhibits no significant monotonic trend ($\tau = -0.13$, $p = 0.34$), supporting its interpretation as a highly oscillatory climate mode rather than a directional driver. Annual cumulative rainfall in Obock is represented in **Figure 5d** and shows no significant monotonic trend ($\tau = -0.011$, $p = 0.95$), indicating strong interannual variability with wetter years post-2015.

Correlation analyses summarized in **Table 1,** reveal the relative influences of climatic and oceanic drivers on mangrove cover and vegetation greenness from 1992 to 2022. For vegetation greenness (NDVI), the

strongest correlation was observed with rainfall measured at Obock ($r = 0.479$, $p = 0.01$), whereas rainfall measured at Djibouti was weaker and non-significant ($r = 0.27$, $p = 0.17$). SLA showed a weak, non-significant positive correlation ($r = 0.354$, $p = 0.08$). Mean temperature exhibited a modest negative association with NDVI ($r = -0.30$, $p = 0.03$), while minimum and maximum temperatures were non-significant. Niño 3.4 and IOD indices had no significant correlations with NDVI. For mangrove cover, SLA had the strongest and most significant relationship ($r = 0.62$, $p < 0.001$) indicating that higher sea levels corresponded to increased mangrove area. Obock rainfall showed a weak, marginally positive relationship ($r = 0.28$, $p = 0.05$) with mangrove cover, whereas rainfall measured at Djibouti was non-significant ($r = 0.17$, $p = 0.39$). All temperature metrics (minimum, maximum, and mean), Niño 3.4 and IOD indices had no significant relationships with mangrove canopy cover.

Overall, Obock rainfall and sea level anomaly were the primary hydroclimatic drivers of the Godorya mangrove dynamics. While rainfall showed a stronger association with NDVI variability, SLA had a dominant role in determining the total area of mangroves.

Multiple linear regression (MLR) was performed for NDVI and mangrove cover using detrended anomalies and reported in **Table 2**. The final model accounted for 50.7% of the year-to-year variation in NDVI. The overall fit was statistically very significant with an R-squared of 0.51, an adjusted R-squared of 0.45, an F-statistic of 9.3, and a probability value less than .001. The final model's residuals passed both diagnostic tests ($p=0.39$ for Shapiro-Wilk test; DW statistic = 1.88) confirming there were no violations of normality and/or autocorrelation. The standardized regression coefficient for SLA ($ß=0.49$, $p<.0001$) provided the most direct evidence that SLA positively affects NDVI. Standardized regression coefficients also demonstrated that Obock rainfall ($ß=0.42$, $p=0.0006$) has a positive relationship with NDVI. The final standardized regression equation is:

$$NDVI' = 0.49\,\text{Sea Level Anomaly}' + 0.49\,\text{Obock Rainfall}'$$

The regression model produced better fits for mangrove area than for NDVI. More specifically, for mangrove area the model provided an explanation for a greater amount of year-to-year variation (adjusted R^2 = 0.64; F = 12.9; $p < 0.001$) and thus had more explanatory power. In addition, sea level anomaly ($p < 0.001$) was the most important predictor ($\beta = 0.7$), as it accounted for the largest share of the explained variance. As such, it appears that coastal hydrodynamics has the greatest influence on mangrove extent. A positive association existed between Obock rainfall ($p = 0.008$) and mangrove area while an association with lower magnitude appeared to exist for mean air temperature ($p = 0.025$). The final regression equation is:

$$\text{Mangrove area}' = 0.7\,\text{Sea Level Anomaly}' + 0.39\,\text{Rainfall}' - 0.27\,\text{Mean Temperature}'$$

Discussion

The time-sequenced trajectories of the Godorya mangrove show a non-linear pattern, characterized by an extensive dieback phase (1987–2012) followed by a slight recovery post-2015. Similar non-linear responses have been reported in northern Australia, where the 2015–2016 El Niño event was responsible for a major global mangrove dieback[48,49]. Given the coarse spatial resolution of the climate datasets relative to the spatial extent of the Godorya mangrove, patch climatic variables are interpreted here as providing regional-scale context, while recognizing that local hydrogeomorphic and anthropogenic processes likely modulate within-site variability. However, in both cases, the significant declines in the canopy were associated with anomalously low sea levels combined with drought conditions, demonstrating the relative vulnerability of arid mangroves to compounded hydroclimatic stress. NDVI values of < 0.25 were therefore used as an operational proxy for "very low" photosynthetic activity at a landscape level in this arid mangrove environment, rather than as a physiological mortality threshold. Stressful canopy drought responses with defoliation patterns similar to those described here have been documented in other arid to semi-arid mangrove environments (i.e. Iran and Kenya)[50,51].

Continuous in situ field observations were not available for the 35-year datasets, precluding direct measurements of physiological stress parameters. The recovery of NDVI and mangrove cover was delayed after the decline phase. The absence of a significant monotonic trend in NDVI over the full 1987–2022 period reflects the phase-structured, non-linear trajectory of the system, characterized by a prolonged decline followed by partial recovery rather than a single directional trend. Recovery may be delayed due to physiological recovery processes, the availability of propagules, and the time required for geomorphic conditions to become favorable for forest regeneration[52,53]. This sharp decline around 2001 likely reflects the impact of extreme climatic conditions, potentially associated with the 1997–1998 El Niño event and subsequent environmental stress. As reported for East African mangrove systems, ENSO-associated disturbances can be followed by recovery trajectories spanning a decade or more[54,55]. At Godorya, site-level responses may therefore be partially decoupled from basin-scale indices due to local hydrogeomorphic constraints, time lags, and the coarse resolution of available climate products relative to the mangrove patch. Thus, hydroclimatic parameters are interpreted as providing regional-scale forcing context while hydrogeomorphic configuration and anthropogenic pressure control small-scale mangrove responses within the Godorya system.

Spatial clustering analysis showed that canopy recovery was clustered in the northern depositional areas, while the southern depressions remained persistently degraded. This spatial mosaic illustrates that resilience in Godorya is not spatially uniform, but is mediated by the geomorphic setting. Given established patterns reported for propagation retention and recolonization in the northern intertidal flats of the Gulf of Carpentaria[48], it is plausible that the northern intertidal flats benefited from tidal flushing and sediment accretion. The southern basin, however, where tidal exchange is poor and hypersaline depressions remain, exhibited Low–Low NDVI clusters. Low–Low NDVI clusters may represent ecological traps where natural regeneration is unlikely without active hydrological remediation.

These findings underscore the significance of hydrogeomorphology in mangrove resilience. As recent reviews point out, mangroves at the arid margin are particularly reliant upon sediment supply and tidal connectivity to buffer climatic extremes[16]. In the case of Godorya, where there is no freshwater inflow and negligible sediment supply, the geomorphic position enhances the effects of climatic variability that prevent some areas from meaningfully recovering.

Hydroclimatic drivers are interpreted here as providing regional scale forcing context rather than direct causal controls on mangrove dynamics. In particular, In the case of ENSO (Niño 3.4), it can be considered as a basic form of climate variability that affects the regional hydroclimatic environment; however, there is no statistically significant positive correlation between mangrove cover at Godorya and ENSO or NDVI. Sea-level anomalies and local hydrological conditions instead emerge as the dominant controls on mangrove extent, whereas rainfall primarily modulates short-term canopy greenness through the alleviation of salinity stress. These relationships suggest lagged ecosystem responses to large-scale climate indices. Dieback and recovery may therefore occur when hydrological connectivity and geomorphic conditions allow regeneration[48,56].

This concurs with Mafi-Gholami et al.[50], who found rain pulses could relieve hypersaline stress, but not chronic freshwater depletion. The impact of temperature and IOD were weak, demonstrating that hydrology and sea level anomalies supersede thermal extremes per se, in this hyper-arid environment. The interaction between global (SLA), regional (IOD, rainfall), and local (geomorphology, tidal exchange) influences show that there are multiple scales of mangrove resilience.

These results provide a new understanding of how arid zone systems function at their ecological limits and are consistent with emerging global evidence that extreme climate events will increasingly drive mangrove persistence[48,53]. Northern depositional areas show signs of spontaneous recovery, suggesting that passive or assisted natural regeneration may be

effective where tidal connectivity and sediment dynamics remain functional. Persistently degraded southern depressions are likely constrained by poor hydrological exchange, indicating that recovery in these areas may require targeted hydrological remediation rather than replanting alone. The strong sensitivity of mangrove cover and canopy condition to sea level variability and rainfall pulses further supports the use of arid mangrove systems as sentinels of hydroclimatic stress in the Red Sea–Gulf of Aden region. While this study offers the first long-term analysis of mangrove canopy dynamics in the Godorya MPA, several limitations remain.

4. Limitations

The study relies on NDVI and canopy classification produced by Landsat satellite imagery enable decadal-scale monitoring, which enable multi-decadal monitoring but cannot capture many of the fine-scale physical structure changes in mangroves systems. Mixed-pixel effects are expected to be most pronounced in hypersaline and tidally dynamic zones due to both sensor limitations and environmental heterogeneity. While these factors likely result in conservative NDVI estimates, they do not affect the relative temporal or spatial patterns of mangrove dieback and recovery identified in this study. Future studies should consider temporally consistent classification approaches or trajectory-based methods to reduce false change detection. Additionally, anthropogenic stressors are acknowledged to be a major source of stress in Godorya. However, consistent data quantifying the amount of these stresses during the period of 1987-2022 were not available; therefore, they could not be used as a quantitative predictor and are addressed qualitatively. Finally, the geomorphic setting of Godorya differs significantly from many systems found within the Red Sea-Gulf of Aden; therefore, caution is warranted when applying the results of this study to other mangrove systems. Linear models may not capture nonlinear dynamics, threshold effects, or spatial heterogeneity inherent to mangrove ecosystem responses in arid coastal environments.

Figure captions

Figure 1. Topographical context of the Republic of Djibouti with a highlight (red) on geomorphological and hydrological features of the Godorya Marine Protected Area (GMPA). The map was created by the authors using QGIS version 3.40.11 (QGIS Development Team, 2024; https://qgis.org) from publicly available geospatial datasets.

Figure 2. Long-term trends in total mangrove area (red triangles; left axis) and annual mean NDVI (green circles; right axis) in the Godorya MPA (1987–2022).

Figure 3. Decadal spatiotemporal dynamics of mangrove cover change in the Godorya Marine Protected Area. Panels (a–d) illustrate transitions in mapped mangrove extent between successive periods: (a) 1987–1997, (b) 1997–2007, (c) 2007–2017, and (d) 2017–2022. Green indicates mangrove expansion (growth), red indicates mangrove loss (decline), and grey represents unchanged areas. The map was created by the authors using QGIS version 3.40.11 (QGIS Development Team, 2024; https://qgis.org).

Figure 4. Spatial patterns of NDVI trends (Sen's slope, Mann–Kendall) and Local Moran's I clustering in the Godorya mangrove system. Panel (A) shows Sen's slope of annual NDVI for 1987–2022, indicating the direction and magnitude of long-term canopy change at the pixel level. Panel (B) presents the Mann–Kendall Z statistic, highlighting the strength and significance of monotonic trends. Panels (C) and (D) display Local Moran's I (LISA) cluster maps for 2012 and 2022, respectively, representing degraded and recovery phases. LISA categories include High–High (clusters of high NDVI values), Low–Low (clusters of low NDVI values), High–Low and Low–High (spatial outliers), and non-significant areas.

Figure 5. Temporal variability of key hydroclimatic drivers used in the climate–mangrove analysis (1992–2022). (a) sea level anomaly, (b) Air temperature, (c) El Niño-Southern Oscillation, and (d) Obock rainfall. Blue area represents the drought period using the standardized precipitation index [57].

Table 1: Correlation between mangrove canopy, NDVI and climate drivers (p-value in brackets).

Variable	Mangrove Canopy	(NDVI)
Minimum Temperature	0.2 (0.26)	-0.23 (0.2)
Maximum temperature	-0.15 (0.38)	-0.23 (0.19)
Mean Temperature	0.02 (0.9)	**-0.3 (0.03)**
Nino 3.4 index	0.18 (0.3)	0.22 (0.19)
Indian Ocean Dipole (IOD)	0.07 (0.67)	-0.08 (0.63)
Sea level anomaly	**0.62 (≤0.01)**	**0.35 (0.05**)
Rainfall (Obock)	**0.28 (0.05)**	**0.48** (0.01)
Rainfall (Djibouti)	0.17 (0.39)	0.27 (0.17)

Table 2. Variability of NDVI and canopy cover detredended anomalies using multiple linear regression analyses in relation to hydroclimatic drivers

	Predictor	Coefficient (β)	Standard error	Standardized coefficient (β)	p-value
NDVI	Intercept	4.15	1.01	—	0.0003
	Sea Level anomaly	1.23	0.23	0.49	<0.0001
	Obock rainfall anomaly	0.0029	0.0007	0.42	0.0006
Mangrove cover	Intercept	1305.94	407.82	—	0.0040
	SLA anomaly	831.41	170.82	0.6	<0.0001
	Obock rainfall anomaly	1.25	0.32	0.39	0.0008
	Mean air temperature anomaly	-36.06	13.30	-0.27	0.012

Figure 1.

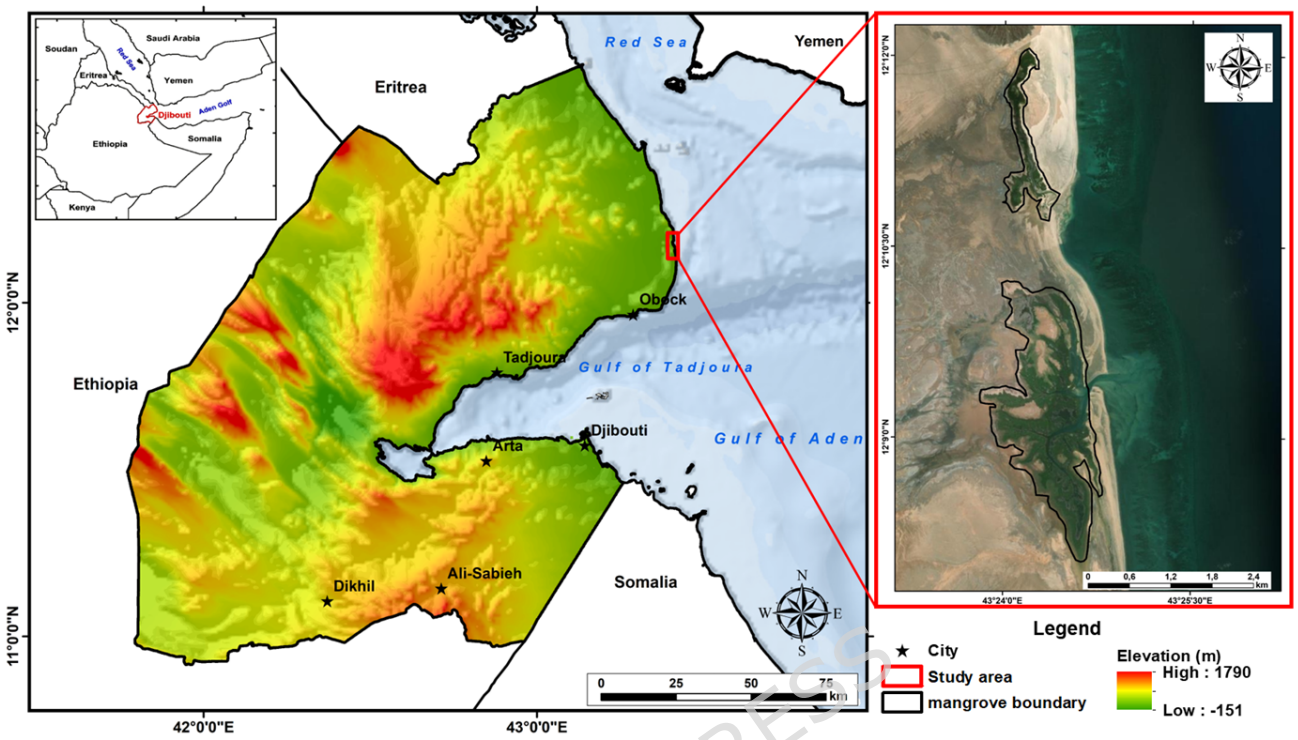

Figure 2.

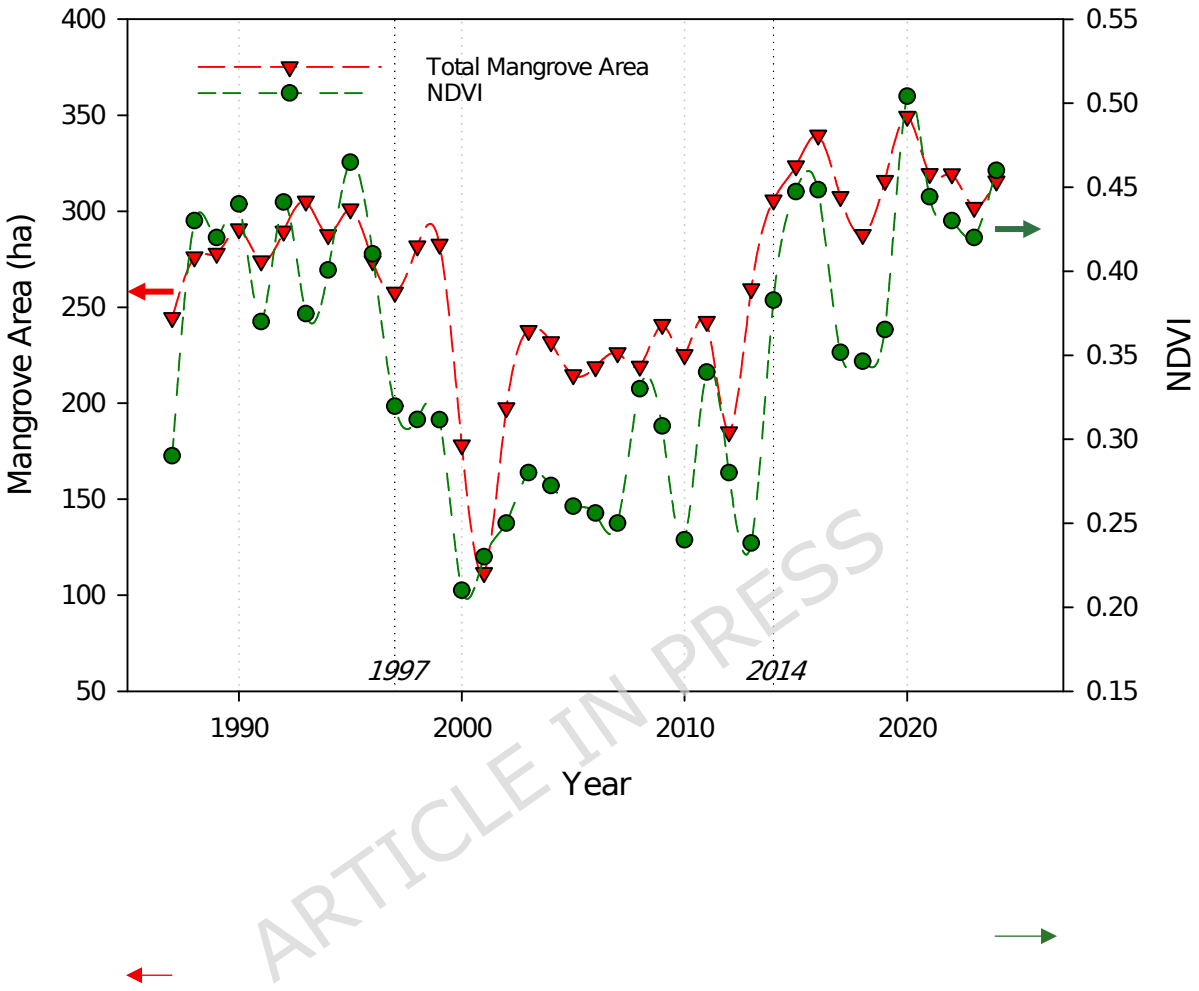

Figure 3.

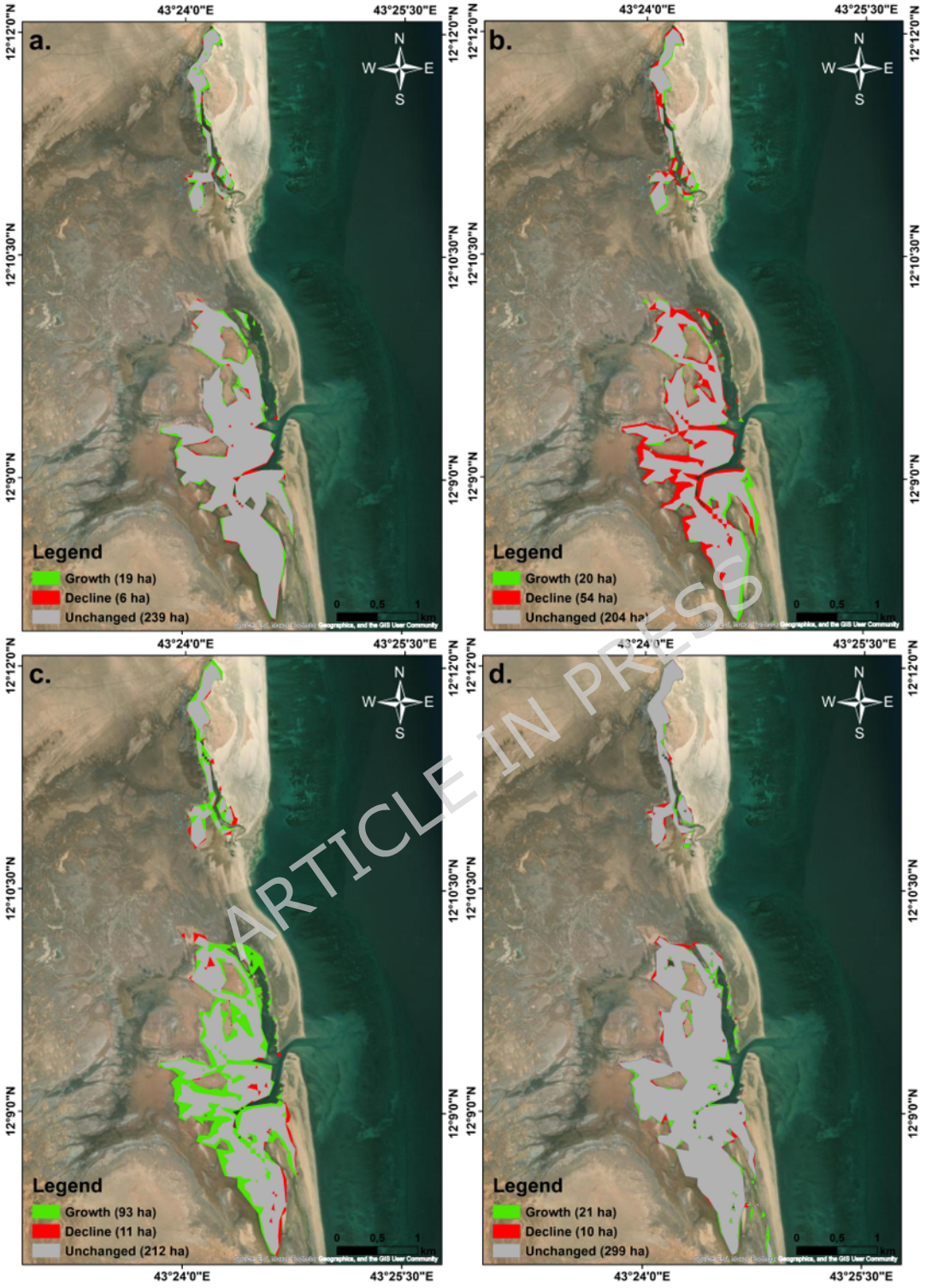

Figure 4.

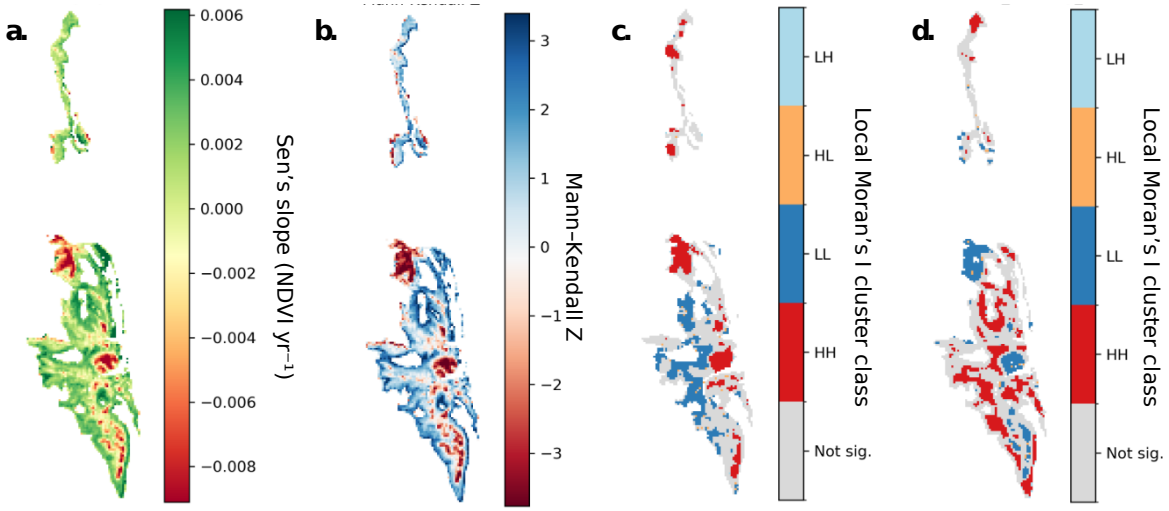

Figure 5.

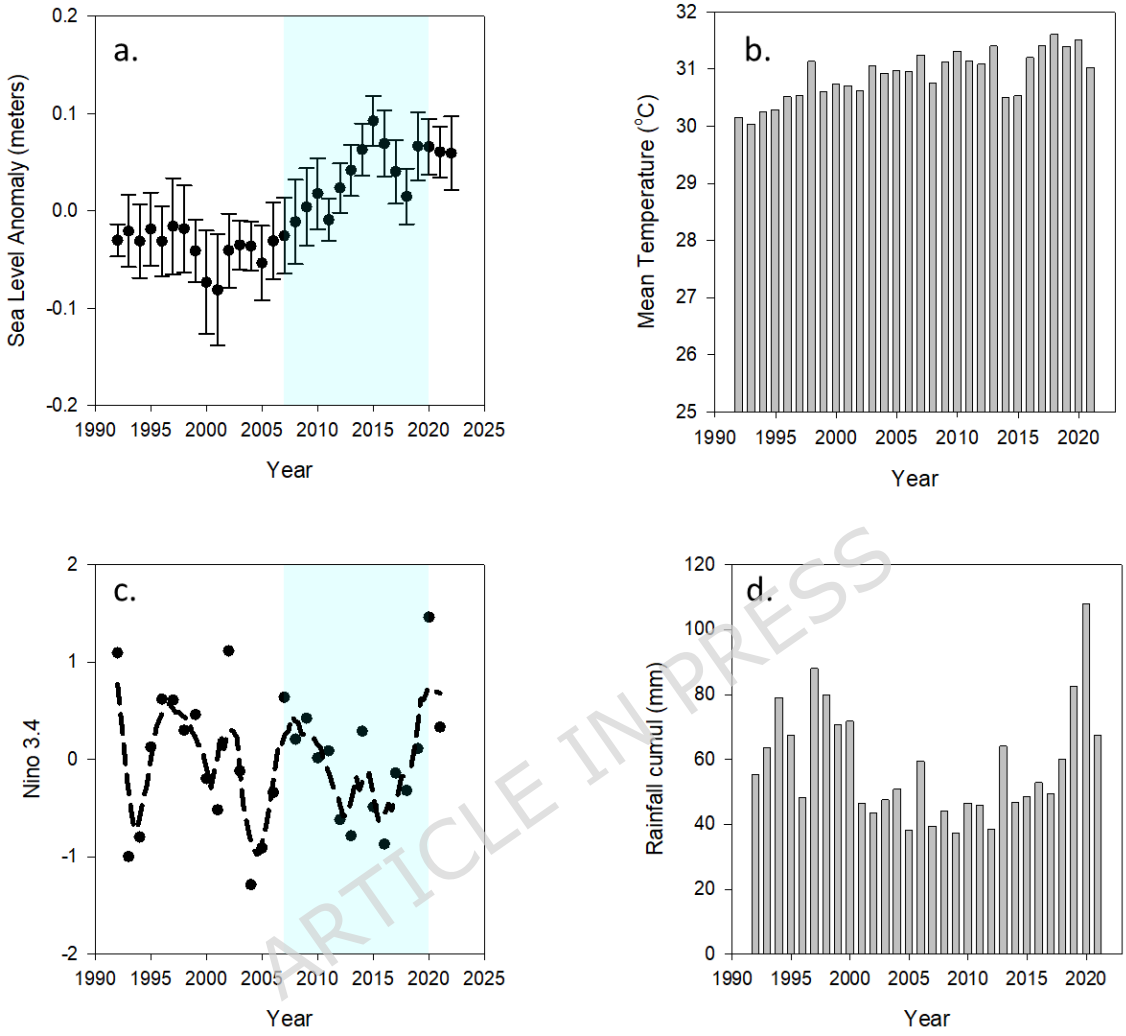

References

1 Kusumaningtyas, M. A. *et al.* Variability in the organic carbon stocks, sources, and accumulation rates of Indonesian mangrove ecosystems. *Estuarine, Coastal and Shelf Science* **218**, 310-323 (2019).

2 Jerath, M. *et al.* The role of economic, policy, and ecological factors in estimating the value of carbon stocks in Everglades mangrove forests, South Florida, USA. *Environmental Science & Policy* **66**, 160-169 (2016).

3 Rao, N. S., Ghermandi, A., Portela, R. & Wang, X. Global values of coastal ecosystem services: A spatial economic analysis of shoreline protection values. *Ecosystem services* **11**, 95-105 (2015).

4 Asari, N., Suratman, M. N., Mohd Ayob, N. A. & Abdul Hamid, N. H. in *Mangroves: Ecology, Biodiversity and Management* 305-322 (Springer, 2021).

5 Marois, D. E. & Mitsch, W. J. Coastal protection from tsunamis and cyclones provided by mangrove wetlands–a review. *International Journal of Biodiversity Science, Ecosystem Services & Management* **11**, 71-83 (2015).

6 Tanaka, N. Vegetation bioshields for tsunami mitigation: review of effectiveness, limitations, construction, and sustainable management. *Landscape and Ecological Engineering* **5**, 71-79 (2009).

7 Cinco-Castro, S., Herrera-Silveira, J. & Comín, F. Sedimentation as a support ecosystem service in different ecological types of mangroves. *Frontiers in Forests and Global Change* **5**, 733820 (2022).

8 Sundaramanickam, A., Nithin, A. & Balasubramanian, T. in *Mangroves: Ecology, Biodiversity and Management* 257-278 (Springer, 2021).

9 Kelleway, J. J. *et al.* Review of the ecosystem service implications of mangrove encroachment into salt marshes. *Global Change Biology* **23**, 3967-3983 (2017).

10 Khalil, A. S. in *The Red Sea: The formation, morphology, oceanography and environment of a young ocean basin* 585-597 (Springer, 2015).

11 Mandura, A. & Khafaji, A. in *Towards the rational use of high salinity tolerant plants: Vol. 1 Deliberations about High Salinity Tolerant Plants and Ecosystems* 353-361 (Springer, 1993).

12 Mohamed, B. F. Ecological observations on mangroves of the Red Sea shores of the Sudan. *Hydrobiologia* **110**, 109-111 (1984).

13 Faye, B. Mangrove, sécheresse et dromadaire. *Science et changements planétaires/Sécheresse* **4**, 47-55 (1993).

14 Mandura, A. A mangrove stand under sewage pollution stress: Red Sea. *Mangroves and Salt marshes* **1**, 255-262 (1997).

15 PERSGA. Status of Mangroves in the Red Sea and Gulf of Aden. 68 (May 2004).

16 Wang, C. Three-ocean interactions and climate variability: a review and perspective. *Climate Dynamics* **53**, 5119-5136 (2019).

17 Maina, J. *et al.* Identifying global and local drivers of change in mangrove cover and the implications for management. *Global Ecology and Biogeography* **30**, 2057-2069 (2021).

18 Osland, M. J. *et al.* Climatic controls on the global distribution, abundance, and species richness of mangrove forests. *Ecological Monographs* **87**, 341-359 (2017).

19 Zhang, Z., Luo, X., Friess, D. A. & Li, Y. Global mangrove growth variability driven by climatic oscillation-induced sea-level fluctuations. *Nature Geoscience*, 1-7 (2025).

20 Friess, D. A., Adame, M. F., Adams, J. B. & Lovelock, C. E. Mangrove forests under climate change in a 2 C world. *Wiley Interdisciplinary Reviews: Climate Change* **13**, e792 (2022).

21 Ghoraba, S. M. M., Almahasheer, H., Siddig, A. A., Nagi, H. M. & Suarez, E. IUCN Red List of Ecosystems, Mangroves of the Red Sea and Gulf of Aden. (2024).

22 Dasari, H. P. *et al.* ENSO influence on the interannual variability of the Red Sea convergence zone and associated rainfall. (2017).

23 Assowe Dabar, O. *et al.* Spatial and temporal variability of rainfall over the Republic of Djibouti from 1946 to 2017. *International Journal of Climatology* **41**, 2729-2748 (2021).

24 Plisnier, P.-D., Serneels, S. & Lambin, E. Impact of ENSO on East African ecosystems: a multivariate analysis based on climate and remote sensing data. *Global Ecology and Biogeography* **9**, 481-497 (2000).

25 Punwong, P., Selby, K. & Marchant, R. Holocene mangrove dynamics and relative sea-level changes along the Tanzanian coast, East Africa. *Estuarine, Coastal and Shelf Science* **212**, 105-117 (2018).

26 Manatsa, D., Chipindu, B. & Behera, S. K. Shifts in IOD and their impacts on association with East Africa rainfall. *Theoretical and applied climatology* **110**, 115-128 (2012).

27 Giri, C. Observation and monitoring of mangrove forests using remote sensing: Opportunities and challenges. *Remote Sensing* **8**, 783 (2016).

28 Aljahdali, M. O., Munawar, S. & Khan, W. R. Monitoring mangrove forest degradation and regeneration: Landsat time series analysis of moisture and vegetation indices at Rabigh Lagoon, Red Sea. *Forests* **12**, 52 (2021).

29 Bardou, R., Friess, D. A., Gillespie, T. W. & Cavanaugh, K. C. Assessing mangrove cover change in Madagascar (1972–2019): Widespread mangrove deforestation is slowing down. *Global Ecology and Conservation* **53**, e03022 (2024).

30 Guo, Y., Liao, J. & Shen, G. Mapping large-scale mangroves along the maritime silk road from 1990 to 2015 using a novel deep learning model and landsat data. *Remote Sensing* **13**, 245 (2021).

31 Heumann, B. W. Satellite remote sensing of mangrove forests: Recent advances and future opportunities. *Progress in Physical Geography* **35**, 87-108 (2011).

32 Hansen, M. C. & Loveland, T. R. A review of large area monitoring of land cover change using Landsat data. *Remote sensing of Environment* **122**, 66-74 (2012).

33 Binh, N. A. & Hauser, L. T. Mapping mangrove multi-trait functional diversity from satellite observations across dense and fragmented stands using spectral-biophysical derivatives. *Scientific Reports* **15**, 22116 (2025).

34 Vasquez, J., Acevedo-Barrios, R., Miranda-Castro, W., Guerrero, M. & Meneses-Ospina, L. Determining changes in mangrove cover using remote sensing with Landsat images: A review. *Water, Air, & Soil Pollution* **235**, 18 (2024).

35 Zhang, Z., Luo, X., Friess, D. A. & Li, Y. Global mangrove growth variability driven by climatic oscillation-induced sea-level fluctuations. *Nature Geoscience* **18**, 488-494 (2025).

36 El Shaer, H. in *INTERNATIONAL FORUM OF THE QUR'ANIC BOTANIC GARDEN.*

37 BADJI, S. Étude de l'écosystème de mangrove de Godorya. 83 (Ministère de l'Agriculture, de L'Eau, de la Pêche, de l'Elevage Chargé des Ressources Halieutiques (MAEPE-RH), 2016).

38 Abbes, R. Bilan des connaissances acquises sur la faune et la flore sous-marines de la région de Djibouti. (1985).

39 Hering, J. Melanistic Striated Heron Butorides striata in Djibouti. *Bull ABC Vol* **21**, 235 (2014).

40 Hering, J. *et al.* Untersuchungen zur Avifauna der Mangrovenwälder Dschibutis sowie zur Klärung taxonomischer Fragestellungen bei Buntastrild Pytilia melba sowie Haussperling Passer domesticus und Somalisperling Passer castanopterus–erste Ergebnisse. *Vogelwarte* **58**, 349-362 (2020).

41 McGrady, M., Rayaleh, H., Dara, A. & Abdillahi, E. Migration of raptors across the Bab el Mandeb Strait, Djibouti, March 2013. *Bulletin of the African Bird Club* **21**, 64-71 (2014).

42 Roy, D. P. *et al.* Characterization of Landsat-7 to Landsat-8 reflective wavelength and normalized difference vegetation index continuity. *Remote sensing of Environment* **185**, 57-70 (2016).

43 Cai, Z., Jönsson, P., Jin, H. & Eklundh, L. Performance of smoothing methods for reconstructing NDVI time-series and estimating vegetation phenology from MODIS data. *Remote Sensing* **9**, 1271 (2017).

44 Cleveland, W. S. & Devlin, S. J. Locally weighted regression: an approach to regression analysis by local fitting. *Journal of the American statistical association* **83**, 596-610 (1988).

45 Sewilam, H., Hassan, B. & Khalil, B. Spatiotemporal distribution of mangrove along the Egyptian Red Sea coast and analysis of hydrological impact on growth patterns. *International Journal of Environmental Science and Technology* **22**, 725-742 (2025).

46 Zhang, Z., Ahmed, M. R., Zhang, Q., Li, Y. & Li, Y. Monitoring of 35-year mangrove wetland change dynamics and agents in the sundarbans using temporal consistency checking. *Remote Sensing* **15**, 625 (2023).

47 Bera, S. & Das Chatterjee, N. Mapping and monitoring of land use dynamics with their change hotspot in North 24-Parganas district, India: A geospatial- and statistical-based approach. *Modeling Earth Systems and Environment* **5**, 1529-1551 (2019).

48 Asbridge, E., Lucas, R., Ticehurst, C. & Bunting, P. Mangrove response to environmental change in Australia's Gulf of Carpentaria. *Ecology and evolution* **6**, 3523-3539 (2016).

49 Lymburner, L. *et al.* Mapping the multi-decadal mangrove dynamics of the Australian coastline. *Remote Sensing of Environment* **238**, 111185 (2020).

50 Mafi-Gholami, D., Mahmoudi, B. & Zenner, E. K. An analysis of the relationship between drought events and mangrove changes along the northern coasts of the Pe rsian Gulf and Oman Sea. *Estuarine, Coastal and Shelf Science* **199**, 141-151 (2017).

51 Verheyden, A., De Ridder, F., Schmitz, N., Beeckman, H. & Koedam, N. High-resolution time series of vessel density in Kenyan mangrove trees reveal a link with climate. *New phytologist* **167** (2005).

52 Van der Stocken, T. *et al.* Impact of landscape structure on propagule dispersal in mangrove forests. *Marine Ecology Progress Series* **524**, 95-106 (2015).

53 Hauser, L. T. *et al.* Uncovering the spatio-temporal dynamics of land cover change and fragmentation of mangroves in the Ca Mau peninsula, Vietnam using multi-temporal SPOT satellite imagery (2004–2013). *Applied Geography* **86**, 197-207 (2017).

54 Erftemeijer, P. L. & Hamerlynck, O. Die-back of the mangrove Heritiera littoralis dryand, in the Rufiji Delta (Tanzania) following El Nino floods. *Journal of Coastal Research*, 228-235 (2005).

55 M'rabu, E., Bosire, J. O., Cannicci, S., Koedam, N. & Dahdouh-Guebas, F. in *Meeting on Mangrove ecology, functioning and Management (MMM3) 2-6 July 2012, Galle, Sri Lanka.* 104.

56 Gitau, P. N., Duvail, S. & Verschuren, D. Evaluating the combined impacts of hydrological change, coastal dynamics and human activity on mangrove cover and health in the Tana River delta, Kenya. *Regional Studies in Marine Science* **61**, 102898 (2023).

57 Assowe Dabar , O. *et al.* Evolution and Trends of Meteorological Drought and Wet Events over the Republic of Djibouti from 1961 to 2021. *Climate* **10**, 148 (2022).

Acknowledgements
The authors gratefully acknowledge the Préfecture d'Obock for facilitating field activities. We also sincerely thank La Marine Nationale for providing logistical assistance during fieldwork. We thank the anonymous reviewers for their constructive comments, which helped to significantly improve the quality and robustness of the manuscript.

Data Availability
The datasets generated and/or analyzed during the current study are available from the corresponding author on reasonable request.

Funding
The authors declare that no external funding was received for this study.